

Pseudo-Fourier Imaging (PFI): A Technique for Spatial Encoding in MRI

Yasser M. Kadah and Xiaoping Hu,* *Member, IEEE*

Abstract—In magnetic resonance imaging (MRI), spatial discrimination is usually achieved with selective excitation and/or Fourier encoding. While these approaches are favorable in most situations, it is sometimes desirable to have an approach that takes advantage of both selective excitation and Fourier encoding. In this paper, we describe the theory and experimental results of a new technique, which we will call pseudo-Fourier imaging (PFI), that provides a flexible combination of both approaches. The technique is based on a windowed Fourier transform that expands the continuous object spatial distribution in terms of coherent states. A detailed description of the proposed technique is presented in this paper. The practical implementation of this technique is described and shown to be achievable using a set of selective excitations combined with a number of Fourier encoding steps. Then, the signal-to-noise ratio of the new technique is derived to show that it can be varied at will anywhere in the range between the ratios for selective excitation and Fourier encoding. Finally, the experimental results of implementing the technique are presented and some potential applications of the technique such as volume imaging, dynamic imaging and magnetic resonance angiography are discussed.

Index Terms—Fast imaging, Fourier imaging, MRI, selective excitation.

I. INTRODUCTION

In magnetic resonance imaging (MRI), spatial localization is achieved using selective excitation or Fourier encoding. These two approaches have rather different, sometimes complementary, characteristics. Selective excitation is realized by applying a bandlimited radio frequency (RF) pulse in the presence of a slice selection gradient. The spatial resolution attainable with this technique is determined by the slice profile which is a direct function of the slice selection gradient strength and the shape of the RF pulse. In forming an image based on selective excitation (e.g., line scanning), data are acquired using multiple localized excitations each affecting a different region of the imaged field of view. Hence, RF excitations can be interleaved within the same repetition time,

TR , for added efficiency. Moreover, it is possible to update the image locally with few excitations to follow dynamic events occurring in a portion of the field of view. Nevertheless, since each region is excited separately, the signal-to-noise ratio (SNR) can be rather low since no data averaging is implicitly incorporated in this process.

On the other hand, Fourier encoding achieves spatial localization through spatial frequency or phase encoding, while the entire volume of interest is excited. By applying varying amounts of Fourier encoding (phase-encoding steps) to sufficiently sample the k -space region of interest, the field of view can be reconstructed using a Fourier transform operation. This means that the resolution in this case is in principle unrestricted while keeping an excellent SNR as a direct result of the implicit averaging in the Fourier transform operation. Since the entire field of view is excited each time, the technique is however susceptible to partial saturation as a function of the time interval between excitations. Moreover, the global nature of Fourier encoding lacks the desirable spatial localization property, making it necessary to reacquire the entire data set to update any portion of the image.

The differences between selective excitation and Fourier encoding are well recognized and have been carefully taken into consideration in various applications. For example, in volume imaging, multislice imaging takes advantage of the interleaving capability of selective excitation to efficiently collect images with high contrast, while three-dimensional (3-D) acquisition is routinely used to obtain high-resolution, high-SNR images. In certain applications, the use of either one of these two techniques may not be optimal and a combination of the two methods may in fact be desired. For example, in time-of-flight (TOF) magnetic resonance angiography (MRA) [(TOF MRA)], the tradeoff between SNR, slice thickness, and contrast makes it suboptimal to use either multislice or 3-D acquisition. This motivates the introduction of hybrid techniques to combine features from both techniques. For example, in multiple overlapping thin slab acquisition (MOTSA) [1], the volume of interest is scanned via the acquisition of a number of slabs, each acquired in a 3-D fashion while the different slabs are covered in a multislice fashion. In this case, the thin slabs allowed for good flow contrast while the 3-D encoding within the slabs provided good spatial resolution and an improved SNR ratio. In spite of the success of such hybrid techniques, they are limited by their data inefficiency arising from slab overlapping (as much as 50%). Therefore, a technique that allows smooth and flexible combination of the characteristics of selective excitation and

Manuscript received January 14, 1997; revised August 8, 1997. This work is supported in part by the National Institutes of Health under Grants RR08079 and MH55346 and the Islamic Development Bank Merit Scholarship Programme. The Associate Editor responsible for coordinating the review of this paper and recommending its publication was Z.-P. Liang. *Asterisk indicates corresponding author.*

Y. M. Kadah is with the Department of Radiology, Center for Magnetic Resonance Research, and Biomedical Engineering Program, University of Minnesota, Minneapolis, MN 55455 USA

*X. Hu is with the Department of Radiology, Center for Magnetic Resonance Research, and Biomedical Engineering Program, University of Minnesota, 385 East River Road, Minneapolis, MN 55455 USA (e-mail: hu@sparky.drad.umn.edu).

Publisher Item Identifier S 0278-0062(97)09346-4.

Fourier encoding while acquiring the data efficiently can be advantageous.

More recently, the application of MRI has been extended to interventional and dynamic imaging studies. In most of these applications, only a localized region needs to be updated rapidly. Such applications inspired the development of several novel encoding techniques such as wavelet encoding [2] and singular value decomposition (SVD)-based encoding [3]. Nevertheless, problems in the practical implementation and use of these techniques for actual clinical applications hindered such techniques from becoming realistic alternatives. For example, the need to accurately generate many different excitation profiles in both techniques is difficult in practice especially when the profiles are rather localized. Therefore, a spatial encoding technique that allows for fast localized image updating while keeping a simple implementation procedure is desirable for such applications.

In this paper, the problem of magnetic resonance imaging with flexible excitation profiles acquired at a number of phase-encoding steps is considered. In particular, an approach for spatial encoding based on acquiring a set of windowed Fourier transform (WFT) coefficients is developed. This procedure is shown to be a general technique representing a flexible hybrid of selective excitation and Fourier encoding. In particular, the proposed technique corresponds to the multislice technique at one extreme and the Fourier encoding technique at the other. The conditions under which the reconstruction process is stable are described demonstrating that its implementation can be readily achieved on the current MRI systems. Finally, the experimental results of implementing the technique on a commercial MRI machine are presented and illustrate an excellent agreement with the derived theory.

II. THEORY

A. Decomposition of Continuous Functions Using Frames

Consider a continuous function $f \in L^2(\mathcal{R})$, where $L^2(\mathcal{R})$ is the Hilbert space of all square integrable functions $\{f|f: \mathcal{R} \rightarrow \mathcal{C}, \int_{-\infty}^{\infty} |f(z)|^2 dz < \infty\}$, \mathcal{R} is the set of real numbers, and \mathcal{C} is the set of complex numbers. A decomposition of this function can be obtained in terms of a set of basis functions that form a *frame* for $L^2(\mathcal{R})$. A frame is defined as a family of functions $\{w_j\}$, $j \in \mathcal{Z}$, the set of integers, in a Hilbert space \mathcal{H} that satisfies the condition: $A\|f\|^2 \leq \sum_{j \in \mathcal{Z}} |\langle f, w_j \rangle|^2 \leq B\|f\|^2$, for all f in \mathcal{H} and with frame bounds $A > 0$ and $B < \infty$ [4]. If the two frame bounds are equal (i.e., $A = B$), the frame is called a *tight* frame [8].¹ An interesting class of frames is the one generated from a single function $w(z) \in L^2(\mathcal{R})$ (often called the basic window) by translation and modulation in the form $\{w_{m,n}(z) = \exp(j2\pi k_m z) \cdot w(z - z_n)\}$. Examples of such functions are the Weyl–Heisenberg coherent states, which have several applications in quantum physics [5]. When $k_m = mk_o$ and $z_n = nz_o$ for $m, n \in \mathcal{Z}$, the set of integers, and $0 < k_o z_o \leq 1$, these functions form a frame for $L^2(\mathcal{R})$.

¹ It is interesting to note that a frame is different from a basis in that it can admit redundancy in its general form. When a frame is tight with a frame bound $A = 1$ and if $\|w\|^2 = 1$ for all $j \in \mathcal{Z}$, it constitutes an orthonormal basis.

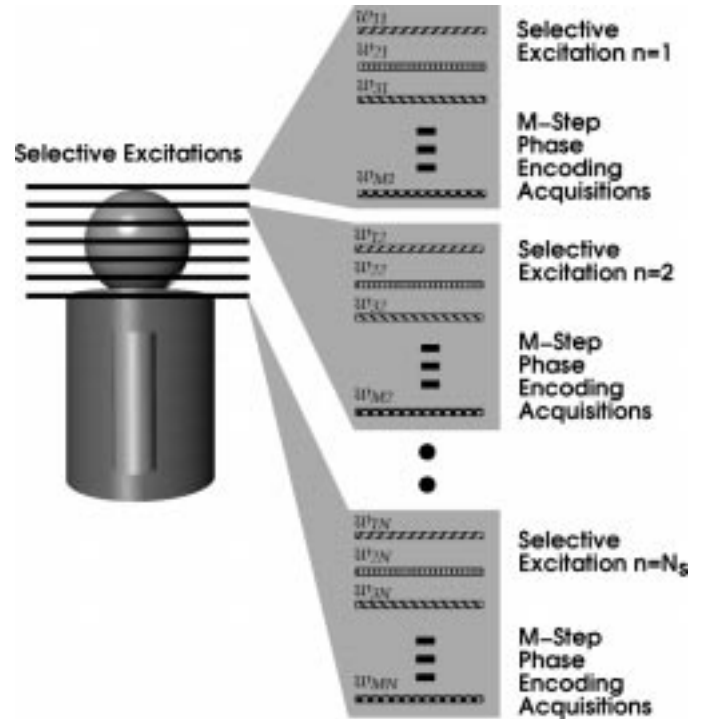


Fig. 1. Data acquisition in PFI. w_{ji} refers to the use of selective excitation window i at phase-encoding step j .

Hence, they can be used to decompose any function in this function space with the WFT defined as

$$\text{WFT}(f)(mk_o, nz_o) = \int_{-\infty}^{\infty} f(z) \cdot w(z - nz_o) \cdot e^{-j2\pi mk_o z} dz. \quad (1)$$

In the special case when the frame functions, w , are derived from a Gaussian function, the WFT is called the *Gabor transform* [6]. More generally, the basic window is frequently a function having compact support in either the frequency domain or the time domain.

The resultant WFT consists of uniform sampling of the phase-space, defined as the Cartesian product of the spatial and spatial-frequency domains, in what is known as the *Gabor lattice* [7]. A stable reconstruction can be computed from the coefficients of this transform provided that the set of window functions composed of the basic window function and its translations and modulations is a frame [5]. In other words, any function $f \in L^2(\mathcal{R})$ can be reconstructed from its WFT decomposition in this case. The technique we present in this paper, the pseudo-Fourier imaging (PFI) technique, reconstructs the object in the slice direction (without loss of generality) by measuring the coefficients of its windowed Fourier decomposition.

B. Pseudo-Fourier Imaging

Consider now the problem of imaging a one-dimensional (1-D) object of transverse spin density $f(z)$ that represents the spin density distribution in the object and the effects of relaxation as a function of the imaging sequence parameters. The signal generated by applying a selective excitation with

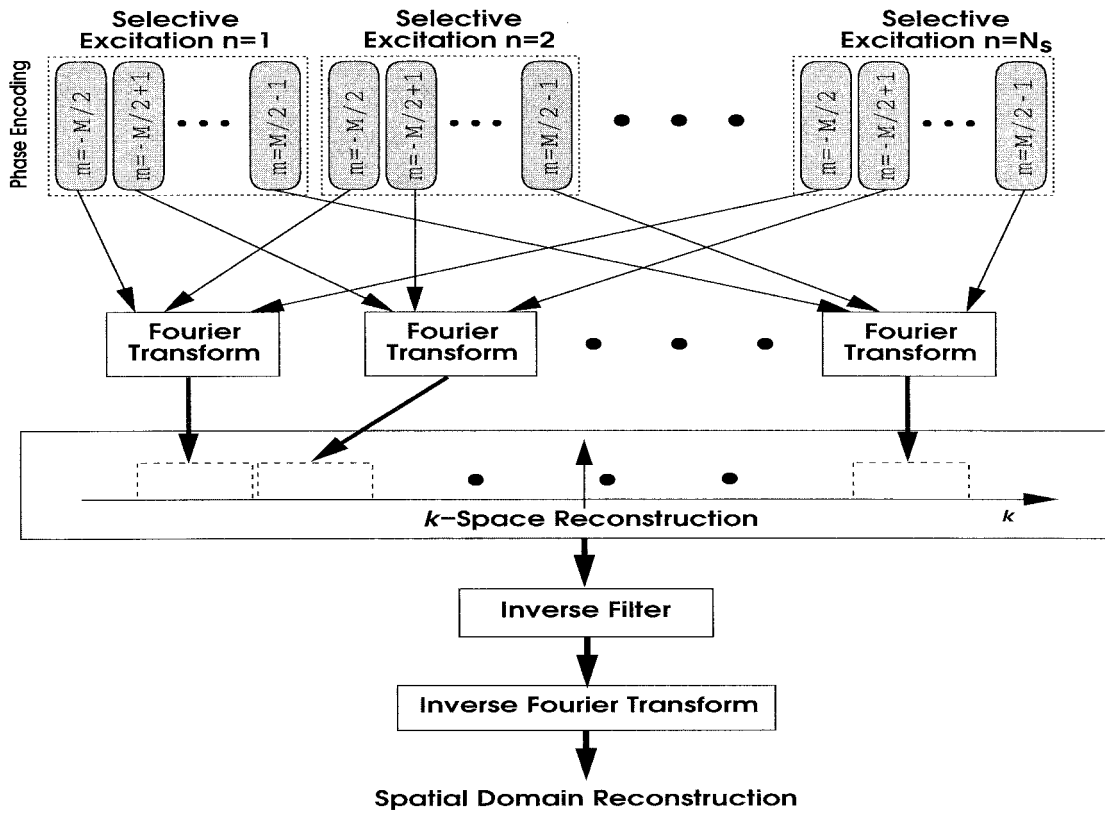


Fig. 2. Block diagram of the 1-D reconstruction procedure in PFI. Starting from the N_s selective excitations acquired at M phase-encoding steps, the reconstruction procedure computes an N -point spatial distribution for the imaged object.

profile $w(z)$ centered at z_n is of the form

$$r_{\text{selective}}(n) = \int_{-\infty}^{\infty} f(z) \cdot w(z - z_n) dz. \quad (2)$$

On the other hand, using a hard pulse to uniformly excite the full extent of the object combined with phase-encoding frequency mk_o yields

$$r_{\text{PE}}(m) = \int_{-\infty}^{\infty} f(z) \cdot e^{-j2\pi mk_o z} dz. \quad (3)$$

Hence, when a selective excitation centered at z_n is combined with a phase-encoding step m , the resultant signal takes the form

$$r_{m,n} = \int_{-\infty}^{\infty} f(z) \cdot w(z - z_n) \cdot e^{-j2\pi mk_o z} dz. \quad (4)$$

In other words, the measured signal is the WFT coefficient corresponding to translation n and modulation m of the basic window $w(z)$. As a result, by properly choosing the selective excitation profile such that the basic window and its translations and modulations form a frame for $L^2(\mathcal{R})$, the object spatial distribution can be reconstructed. An important observation that should be noted here is that the acquired coefficients are exactly the result of the continuous integration form, not of a discrete approximation.

Hence, to apply the theory, RF excitation functions are chosen to be members of the class of functions with spatial profiles $w(z - nz_o)$, where $w(\cdot)$ is a basic window, z_o is the separation distance between neighboring selective excitations,

and n takes the values $1, 2, \dots, N_s$. In other words, these excitations have spatial profiles that represent repetitions of the same excitation profile with different positional shifts. Equation (4) can be expressed in the form of a convolution as

$$r_{m,n} = r_m(z_n) = (f_m * w_R)(z_n) \quad (5)$$

where $f_m(z) = f(z) \cdot e^{j2\pi mk_o z}$, and $w_R(z) = w(-z)$ is the reflection of the window function. Then, given an infinite number of samples $r_m(z_n)$, indexed by n , and assuming that f and w have compact support, a Fourier series can be computed with respect to z_n to obtain

$$R_m(k) = F(k + k_m) \cdot W(-k). \quad (6)$$

Here, $F(\cdot)$ is the Fourier transform of the signal intensity, $W(\cdot)$ is the Fourier transform of $w(\cdot)$ ignoring a multiplicative constant, and $k_m = mk_o$ is the spatial frequency of the phase-encoding frequency step m . Hence, if the excitation profile $w(\cdot)$ has a compact support, $R_m(k)$ will essentially be a windowed version of the original Fourier transform of the object. Moreover, it can be seen that the effect of phase encoding k_m in this formula is to shift the center of this k -space window to scan different parts of the k -space. Hence, by properly selecting the number and step of phase encoding such that the translates of the Fourier transformed windowing function cover the z k -space interval of interest, $F(k)$ can be

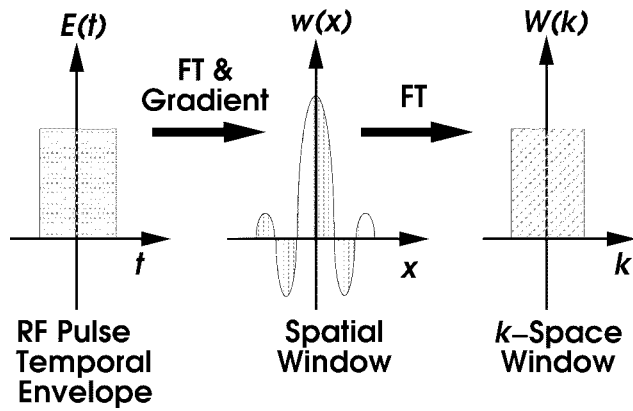


Fig. 3. Excitation profiles for PFI. A rectangular excitation pulse yields a Sinc profile in the spatial domain which in turn provides a rectangular window of the k -space of the imaged object.

computed from

$$F(k) = \frac{\sum_{m=1}^M R_m(k - k_m)}{\sum_{m=1}^M W(-k + k_m)} \quad (7)$$

where M is the number of phase-encoding steps. The condition that guarantees the validity of (7) is that the basic window and its translations and modulations form a frame to $L^2(\mathcal{R})$. Moreover, it is possible to reconstruct a limited k -space representation of the object by acquiring a finite set of the WFT coefficients to uniformly cover the phase-space area of interest. It should be noted that this reconstruction is a special case of the general framework described by Daubechies [8]. In practice, when a finite N_s is used, a discrete Fourier transform (DFT) instead of a complete Fourier series is used, generating $F(k)$ on a discrete grid determined by the Nyquist criteria. The implication of this approximation is addressed in Section VII.

Block diagrams of the data acquisition and the 1-D reconstruction procedure of PFI are shown in Figs. 1 and 2. The data are collected using N_s selective excitations combined with M phase-encoding steps. The points from different selective excitations collected at the same phase-encoding step m [which correspond to $r_m(z_n)$ in the derivation] are put together and passed through a Fourier transformation stage to obtain $R_m(k)$. By collecting the contributions from different phase-encoding steps and passing the outcome through an inverse filter representing the denominator of (7), the spatial distribution of the object is computed by applying an inverse Fourier transformation.

C. Formal Reconstruction Stability Conditions

It is important here to state and discuss the formal conditions under which the above procedure is valid and the reconstruction is stable. First, in (7), to be able to invoke a DFT approximation of the Fourier series without encountering aliasing problems, the sampling along z should satisfy the Nyquist condition. This requirement is clearly determined by the basic window used in the data acquisition, not the extent of

the k -space to be covered in the reconstruction. Given that the received signal is actually a windowed version of the original Fourier transform of f , the sampling scheme is dictated by this much narrower spectrum. The second validity condition is that the set of windows used in the reconstruction form a frame for $L^2(\mathcal{R})$. It can be shown that this condition is satisfied when $k_o \cdot z_o \leq 1$ and the combined support of the basic window and its translations in either the time or the frequency domains forms a complete cover to the real line in that domain [5]. This condition can be alternatively visualized from the fact that the reconstruction formula will have poles when the support of the denominator contains some “holes.” It should be noted that this condition does not require the support of the different shifts of the basic window to be nonoverlapping, i.e., their union being what could be termed a *tight* cover of the real line \mathcal{R} corresponding to the spatial frequency. Nevertheless, any degree of overlapping is an inefficiency in the implementation since some parts of the k -space will be covered more than once during the data acquisition. This translates into extra acquisition time since more phase-encoding steps will be needed to form the k -space cover. An efficient implementation should, therefore, be as close as possible to a tight cover.

III. EXAMPLE OF APPLYING PFI THEORY

As an example of the above theory, let us now consider the case when a square pulse is used. That is, the basic RF excitation envelope function is given by

$$E(t) = \begin{cases} 1 & \text{for } |t| \leq \tau/2 \\ 0 & \text{for } |t| > \tau/2 \end{cases} \quad (8)$$

where τ is the temporal support of the pulse. The spatial profile $w(z)$ of this excitation is approximately a Sinc function peaked at the slice location for flip angles below 30° . In this case, the k -space window $W(k)$ of PFI approximately takes the form of a rectangular window as shown in Fig. 3. To assess the validity of this approximation, the slice profiles were computed from the exact solution of the Bloch equations [9] for the above RF excitation at different flip angles and the results are shown in Fig. 4. The corresponding k -space window shapes of PFI computed by Fourier transforming the excitation profiles are shown in Fig. 5. The k -space window profiles in Fig. 5 are provided to show the limitations of the ideal profiles and to illustrate the form of the nonideality beyond this limit, which is necessary to derive the denominator in (7). As can be seen, the approximation of a Sinc excitation profile and a rectangular k -space window asserted above is valid. The spatial frequency span of the excited profile is approximately equal to $\gamma \cdot G \cdot \tau$, where γ is the gyromagnetic ratio and G is the slice selection gradient in use.

Suppose now that we would like to obtain a bandlimited k -space approximation of the imaged object within $\pm \text{BW}_{\max}/2$, where BW_{\max} is the bandwidth of interest. To satisfy the reconstruction stability conditions, the support of the excitation τ should be related to the number of required phase-encoding steps M as

$$M \cdot (\gamma \cdot G \cdot \tau) \geq \text{BW}_{\max} \text{ or } \tau \geq \frac{\text{BW}_{\max}}{M \cdot \gamma \cdot G} \quad (9)$$

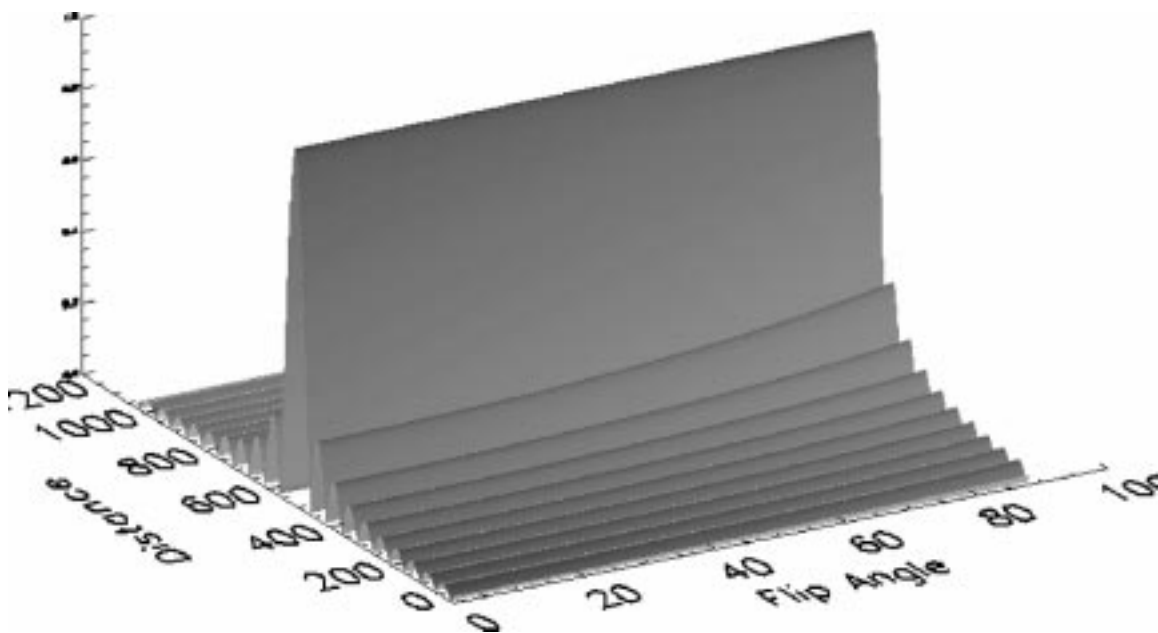


Fig. 4. PFI spatial excitation profiles using a rectangular RF pulse at different flip angles. The deviation from the ideal Sinc profile is evident at high flip angles.

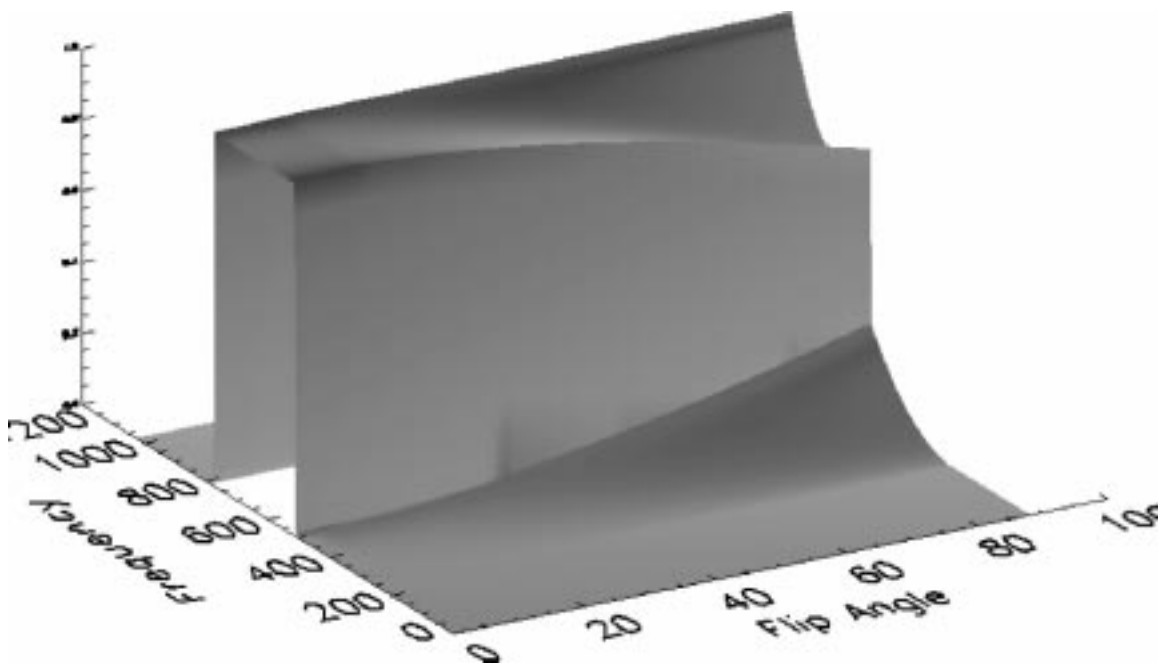


Fig. 5. PFI k -space windows when a rectangular RF pulse is used at different flip angles. The ideal rectangular shape is possible to achieve only at low flip angles.

The spacing of acquired selective excitations should satisfy the Nyquist criterion for spatial frequency bandwidth $\gamma \cdot G \cdot \tau$, i.e., $N_s/L \geq \gamma \cdot G \cdot \tau$. Consequently, the required number of selective excitations N_s for an object of length L is given by

$$N_s \geq \text{ceiling} \left\{ \frac{L \cdot \text{BW}_{\max}}{M} \right\}. \quad (10)$$

The object's Fourier transform is constructed by concatenating segments of it from different excitations as shown in Fig. 2. It is worth noting that in the above example the coverage of the k -space can be made *tight*. In this case, all parts of the

k -space are acquired only once, making this implementation most efficient in acquisition time.

IV. SIGNAL-TO-NOISE RATIO OF PFI

Now let us consider the SNR ratio in the tight cover case of the new technique. This particular case was selected to avoid the implicit averaging effects encountered in the general form of the technique due to multiple acquisitions of the same data, thus allowing the direct comparison with conventional Fourier imaging. In this case, the reconstruction formula can be put

in the form

$$F(k) = \sum_{m=1}^M H(-k + k_m) \cdot R_m(k - k_m) \quad (11)$$

where $H(k)$ is an inverse filter function that has the same support as $W(k)$ and is equal to its reciprocal within that support. We will assume that the only source of noise is the random noise arising from the combined resistance of the imaged subject and the receiver coil. Assuming that N_s selective excitations at M phase-encoding steps are acquired to reconstruct $N = N_s \times M$ points, these samples undergo the following steps in the reconstruction process:

- 1) N_s -point discrete Fourier transform;
- 2) inverse filtering (scaling by constants);
- 3) N -point inverse discrete Fourier transform.

These steps can be described mathematically as follows. First, the acquired samples take the form

$$\hat{r}_m(z_m) = \int_{-\infty}^{\infty} f(z) \cdot w(z - z_n) \cdot e^{-j2\pi k_m z} dz + n_{m,n} \quad (12)$$

where $n_{i,m} \sim \mathcal{N}(0, \sigma^2)$, assumed to be an independent and identically distributed additive zero-mean Gaussian white noise with variance σ^2 . Hence, the noise contamination of different samples are assumed to be uncorrelated. Given the N_s samples obtained at a phase-encoding step m , an N_s -point discrete Fourier transform is applied thus yielding

$$\hat{R}_m(k) = \mathbf{DFT}\{\hat{r}_m(z_n)\} = F(k + k_m) \cdot W(-k) + \tilde{n}_{k,m} \quad (13)$$

where $\tilde{n}_{k,m} \sim \mathcal{N}(0, N_s \sigma^2)$. Since the discrete Fourier transform is an orthogonal transformation, $\tilde{n}_{k,m}$ values are uncorrelated.

The next step in the reconstruction process is the possible use of inverse filtering to restore k -space window shapes to the rectangular shape. The measured k -space window can deviate from a rectangle either by the choice of desired k -space window or due to RF pulse nonlinearity for large flip angles ($>30^\circ$) in a square pulse implementation. This process can be expressed as

$$\bar{R}_m(k) = \hat{R}_m(k) \cdot H(-k) = F(k + k_m) + \bar{n}_{k,m}. \quad (14)$$

Now the noise term becomes $\bar{n}_{k,m} \sim \mathcal{N}[0, N_s \sigma^2 |H(k)|^2]$. In the ideal case of a rectangular profile, $H(k) = 1$ and $\bar{n}_{k,m} \sim \mathcal{N}(0, N_s \sigma^2)$. Since this step does not involve any mixing of k -space samples, the noise within each of these samples continue to be uncorrelated after inverse filtering.

In the final step, the full k -space is composed by the direct sum of these pieces and an inverse discrete Fourier transformation (**IDFT**) is performed to obtain the final image. That is

$$\begin{aligned} \bar{f}(z) &= \mathbf{IDFT}\{\bar{F}(k)\} = \mathbf{IDFT}\left\{\sum_{m=1}^M \bar{R}_m(k - k_m)\right\} \\ &= f(z) + n'_z \end{aligned} \quad (15)$$

where $M \cdot N_s = N$, the total number of points. Since the noise components in the k -space samples are uncorrelated, the noise in the final image is given as $n'_z \sim \mathcal{N}[0, \sigma^2 \sum_{m=1}^{N_s} |H(k_m)|^2 / (M \cdot N_s)]$ if H is constant on its support. It can be seen that the noise power is independent of the location z and therefore will be uniform in the resultant image. It should be noted the noise in different pixels will be correlated when an inverse filter $H(k) \neq 1$ is applied. Two special cases of interest should be pointed out from the above expression. In the first case of volume imaging where $N_s = 1$ and $M = N$, the noise variance is σ^2/N . On the other hand, for the second special case of selective excitation, $N_s = N$ and $M = 1$ and, therefore, the noise variance is simply σ^2 . These two values mark the two ends of the range of possible values for the noise variance. Other values within this range can be achieved with the choice of N_s and M of the PFI.

Another important ratio that can be computed for PFI is the *efficiency figure of merit*, defined as

$$\eta = \frac{\text{SNR}}{\sqrt{\text{time}}} \quad (16)$$

where *time* refers to the acquisition time. This ratio is used mainly to compare different imaging techniques. For example, when we compare selective excitation to Fourier imaging, we obtain

$$\frac{\eta_{\text{Fourier}}}{\eta_{\text{Selective}}} = \sqrt{N} \quad (17)$$

where imaging times are assumed to be the same for both techniques. Similarly, the comparisons between PFI and these two techniques can be computed as follows:

$$\frac{\eta_{\text{PFI}}}{\eta_{\text{Selective}}} = \sqrt{\frac{N}{\sum_{m=1}^{N_s} |H(k_m)|^2}} \quad (18)$$

and

$$\frac{\eta_{\text{PFI}}}{\eta_{\text{Fourier}}} = \sqrt{\frac{1}{\sum_{m=1}^{N_s} |H(k_m)|^2}}. \quad (19)$$

It should be noted that the efficiency figure of merit described here does not take into account slice interleaving. Therefore, the actual efficiency for selective excitation and PFI may be higher in practice. It is also interesting to see that the tight coverage of the k -space leads to the best efficiency in terms of acquisition time, and not necessarily in terms of the SNR which depends on the shape of the tight coverage.

V. POTENTIAL APPLICATIONS OF PFI

As a general encoding method, PFI can be applied in a number of areas in MRI. In the following, three possible applications are discussed in some detail as examples.

A. Volume Imaging

Currently, volume imaging is performed through either the acquisition of multiple thin slices or phase encoding in the

slice direction. Multiple slice acquisition has the advantage of slice interleaving which allows the use of suitable TR values for proper contrast. On the other hand, multislice imaging suffers from slice profile limitations as well as low SNR. With PFI, interleaving can be used to excite the slabs while keeping Fourier encoding to provide better resolution and SNR. Moreover, the tradeoff between these characteristics can be controlled flexibly through the selection of the number of selective excitations and phase-encoding steps.

B. Magnetic Resonance Angiography (MRA)

In MRA based on time-of-flight contrast, problems are often encountered in association with both two-dimensional (2-D) (multislice) and 3-D (thick volume) approaches. The 2-D acquisition provides excellent flow contrast, but has a limited slice resolution and SNR. On the other hand, while the SNR and slice thickness are not problematic in 3-D acquisition, saturation of the moving spins in the blood from repeated excitations degrades flow contrast. Hence, a hybrid between the two techniques can be advantageous. PFI provides a natural vehicle for such a hybrid technique. It should be noted here that PFI is different from the multiple overlapped thin-slab acquisition (MOTSA) technique which is based on conventional Fourier imaging [1]. Moreover, MOTSA suffers from a high degree of redundancy in data acquisition as a result of overlapping between consecutive slabs. In contrast, PFI can be implemented without any redundancy in data acquisition.

C. Simultaneous Space/ k -Space Localization

An important property of PFI is its ability to represent events that are localized in both image space and k -space. This is particularly of interest in such applications as dynamic imaging. Many authors have suggested different methods of reduced data acquisition, either in the k -space or the spatial domain [10], [11]. The objective of these methods is to obtain fast updates of the dynamic information within a given image. Wavelet encoding can be potentially used to limit the dynamic information in both domains [2]. However, its implementation is cumbersome, if not impractical, for many reasons [12], [13]. For example, the need to generate very thin excitation profiles is difficult in practice in addition to its prohibitively low SNR. From the above description of the pseudo-Fourier technique, it can be seen that PFI readily permits reduced data acquisition in both domains. For example, to reduce the updated k -space data, one can acquire only the low phase-encoding steps. On the other hand, when the dynamic event is known *a priori* to be localized to within only a small portion of the image, one can limit the number of updated selective excitations. In this case, the pseudo-Fourier technique will only acquire those selective excitations that are localized around the dynamic object, providing a better temporal resolution for the dynamic imaging sequence.

VI. EXPERIMENTAL VERIFICATION OF PFI

To experimentally demonstrate the new technique, PFI was implemented on a 1.5-T SIEMENS Magnetom Vision MR scanner (SIEMENS Medical Systems, Erlangen, Germany).

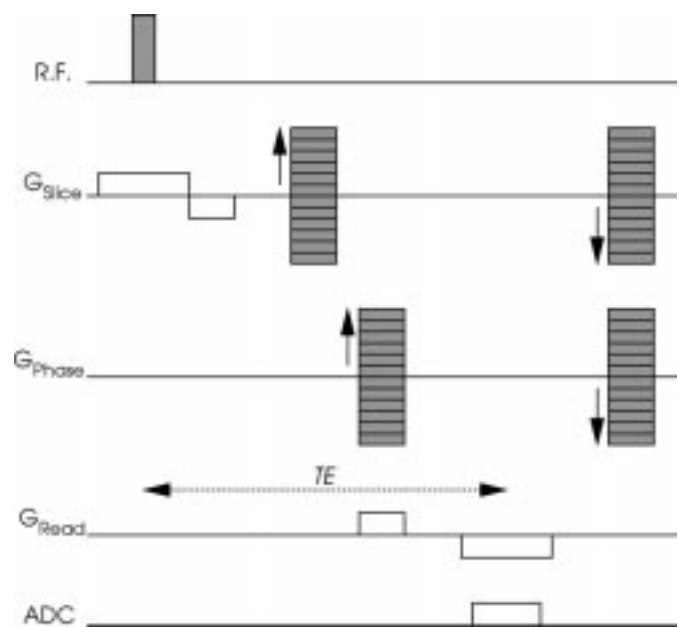


Fig. 6. A diagram of the 3-D pulse sequence used to implement PFI in the slice direction.

Volume data were acquired for a standard resolution phantom in which the PFI technique was used to reconstruct the slice direction. A diagram of the pulse sequence used is shown in Fig. 6. The data were obtained using a FLASH sequence [15] with a nominal flip angle α of 25° , a TR of 15 ms, and a TE of 6 ms. A $512\text{-}\mu\text{s}$ square excitation pulse profile was used in the presence of a 2.9-mT/m gradient for selective excitation. The number of acquired selective excitations (N_s) was 19 and they were 16 mm apart. In addition to the in-plane encoding ($25.6\text{-cm} \times 25.6\text{-cm}$ FOV and 256×96 matrix), the number of phase-encoding steps along the slice direction for the pseudo-Fourier technique (M) was 16. The data were then used to reconstruct a total of 304 slices 1-mm thick using (7). Reformatted images along the PFI and frequency encoding directions from the volume data reconstructed using PFI are shown in Fig. 7 along with a zoomed version to show the 1-mm bars obtained with both PFI and conventional 2-D Fourier encoding for comparison in Fig. 8. The pseudo-Fourier technique was used in the horizontal direction. The images exhibit 1-mm resolution in the PFI direction, in agreement with what the PFI theory predicted. The comparison between the two images indicates that the new technique provides a similar resolution as the conventional Fourier encoding. Nevertheless, the flexibility of the new technique in combining desirable features of multislice and volume imaging will be beneficial for many applications.

Examples of using PFI in MRA are shown in Figs. 9 and 10 for effective spatial window thicknesses of 8 and 16 mm, respectively, (i.e., separation distance of translated spatial windows). A volume of $200 \times 200 \times 128\text{ cm}^3$ was covered by a $256 \times 192 \times 128$ matrix with PFI in the third dimension. The total acquisition time in both sequences was 12 min. As can be seen, the smaller window provides better detail while the larger window has a better SNR. The images also exhibited good vessel contrast despite the fact that the sequences are not yet

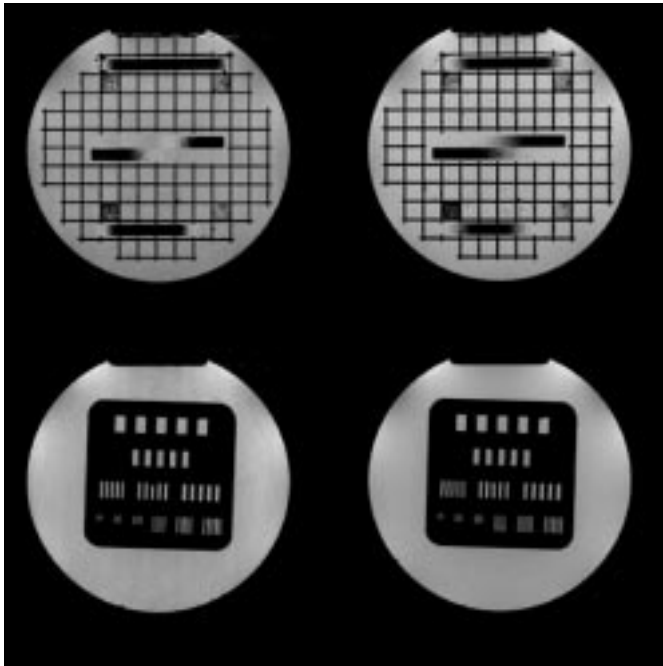


Fig. 7. Experimental result of imaging a resolution phantom with PFI. The PFI images (left) exhibit a similar resolution to the comparison images obtained with Fourier imaging (right) in the PFI direction (horizontal). Imaging parameters were: flip angle α of 25° , a TR of 15 ms, and a TE of 6 ms.

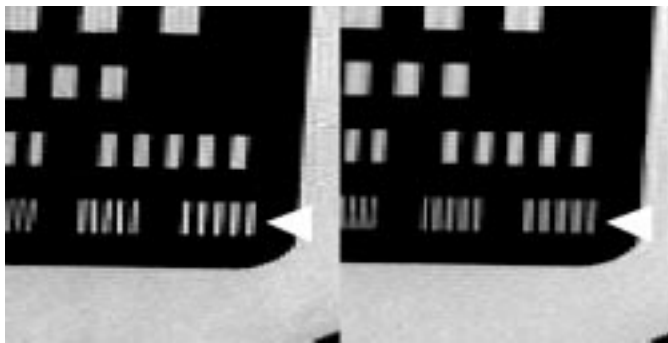


Fig. 8. Zoomed version of the bottom images shown in Fig. 7. PFI was used in the horizontal direction of the left image and is clearly comparable to Fourier imaging used in the right image. This can be particularly seen from the 1-mm resolution bars indicated by the arrow heads.

optimized. Sequence optimization includes the choice of the imaging sequence timing parameters TR and TE , the choice of the spatial window width, and the sequencing of different selective excitations within the 3-D imaging sequence.

To demonstrate the potential of PFI for dynamic imaging applications, the spatial/ k -space localization property is demonstrated in this example. This experiment aimed at illustrating the capabilities of PFI in reconstructing selected portions of an image with a different resolution, chosen to be lower than the rest of the image in this example. Images were reconstructed with various amounts of data omitted to simulate reduced data acquisition. In Fig. 11, different portions (indicated by an arrow) of the images in (b) and (c) were reconstructed using fewer phase-encoding steps. This was done by using only five encoding steps for the selective

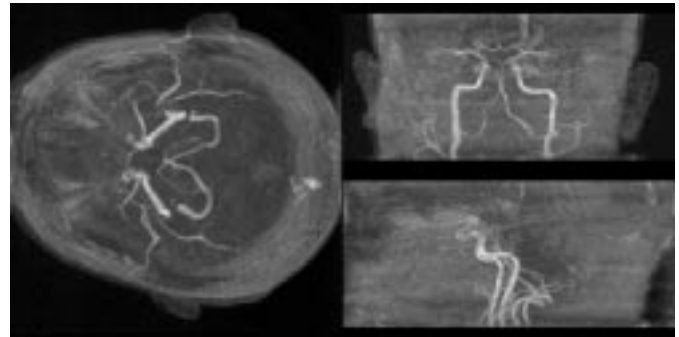


Fig. 9. MIP images obtained with PFI with spatial window size of 8 mm. PFI was used to encode the axial direction (indicated by arrows). Imaging parameters were: flip angle α of 40° , a TR of 15 ms, and a TE of 6 ms. The advantage of PFI is exhibited by the smoothness in the PFI direction and the visualization of small vessels (indicated by black arrow heads).

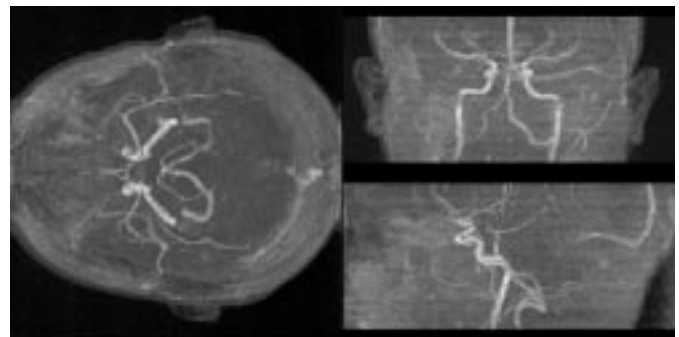


Fig. 10. MIP images obtained with PFI with window size of 16 mm. PFI was applied to encode the axial direction (indicated by arrows). The images are less noisy but provide poorer visualization of small vessels. Imaging parameters were: flip angle α of 40° , a TR of 15 ms, and a TE of 6 ms.

excitations covering these regions while the full data for the other slices was used in the reconstruction. As can be seen, the resultant image exhibits a localized low-resolution portion in the corresponding slice locations. In the case of using five steps for one slice, the image portions corresponding to this slice in the volume of interest can be updated at a rate of 75 ms for each image in the volume. It should also be noted that although a pseudo-Fourier encoding was applied in the slice direction, it can be applied in the phase-encoding direction as was demonstrated for wavelet encoding approaches [2] and the SVD [3].

VII. DISCUSSION

To illustrate the hybrid nature of PFI, two extreme cases of the technique can be considered. In the first, when the excitation profile covers the entire volume, the technique becomes equivalent to the conventional Fourier volume imaging. In this case, the number of points in the PFI reconstruction is equal to the number of phase-encoding steps ($N = M$) with a single slice ($N_s = 1$). This represents the approach in volume imaging where the k -space is sampled by phase encoding. On the other extreme, when the excitation profile is very thin, PFI corresponds to the conventional multislice imaging. This is the case when the number of points in the PFI reconstruction is equal to the number of selective excitations ($N = N_s$) with

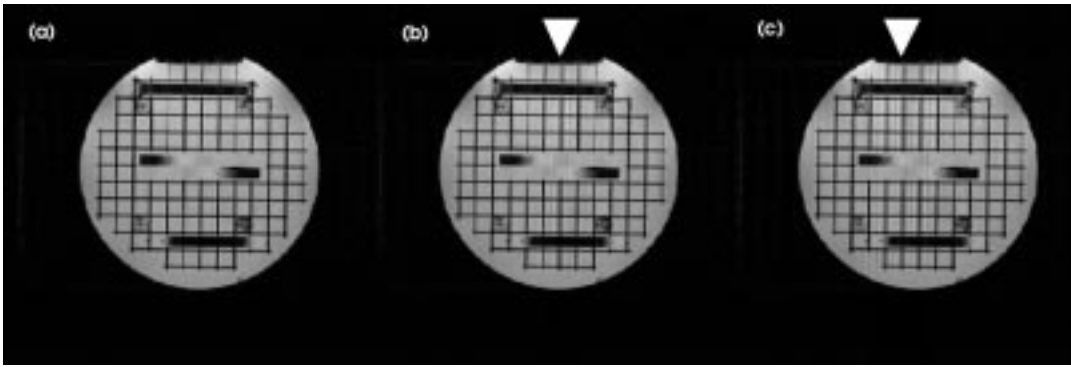


Fig. 11. Example of spatial/ k -space localization capabilities of PFI for potential use in dynamic imaging: (a) full PFI reconstruction, (b) reduced k -space acquisition in one PFI selective excitation, and (c) reduced k -space acquisition in three PFI selective excitations. The arrow heads in (b) and (c) indicate the regions where reduced k -space data acquisition was used. Imaging parameters were: flip angle α of 25° , a TR of 15 ms, and a TE of 6 ms.

no phase encoding applied ($M = 1$). Therefore, by selecting the parameter M , one can move anywhere between these two extreme cases to obtain a tailored hybrid technique for the specific application at hand.

Because the k -space window used in PFI is compact, its spatial representation, i.e., the excitation profile, is infinite in extent. Consequently, the convolution in the right-hand side of (5) also has an infinite spatial extent in principle. In practice, a finite number of selective excitations are used, and therefore only a truncated version of the convolution is sampled. This truncation necessitates the use of a discrete Fourier transform instead of a complete Fourier series. Due to the implicit assumptions of the discrete Fourier transform, the resultant $R_m(k)$ is blurred by the Fourier transform of the finite sampling window. This blurring is usually negligible since the effective support of the convolution is often small.

As an unconventional spatial encoding technique, an interesting comparison arises between PFI and other experimental techniques such as SVD or wavelet encoding. The SVD technique is based on the availability of *a priori* knowledge regarding the object to be imaged [3]. Using this knowledge, it may be possible to determine a reduced set of acquisitions to obtain data relative to a basis that results in images that are closest to the original in a least-squares sense. The main problem for the SVD technique arises from the availability and applicability of the needed *a priori* information [14]. This is especially problematic in applications such as dynamic imaging where the image content may undergo drastic changes in a dynamic event. In other words, the singular values of the dynamic information may not be similar to those of the static images known *a priori*. The pseudo-Fourier technique does not assume such *a priori* description of the imaged object.

Let us now compare PFI with the wavelet encoding technique [2]. The motivation of implementing wavelet decomposition in most of its original applications is to have basis functions maintaining localization properties in both the spatial and k -space domains. This translates into less ringing artifacts in both domains while retaining the completeness and invertibility of the transform. Both wavelet encoding and PFI techniques are based on reconstructing the object through obtaining windowed versions of the object spectrum. The main difference between the wavelet encoding and PFI

is that the phase-space plane in the wavelet encoding is sampled nonuniformly, unlike with PFI where it is uniformly sampled on a Gabor grid. Consequently, the windows used in wavelet encoding are usually overlapping and of different widths, whereas the windows in PFI are constant in width. The variable window width for wavelet encoding makes it difficult to implement and prone to low SNR.

The computational complexity of PFI is estimated to be $O(N \log N)$ flops for reconstructing an N -point line. This estimate is independent of the window shape used (or equivalently the basis functions used) with a possible increase in acquisition time in the case of overlapping windows (over-complete frame). This presents a significant reduction of the reconstruction complexity over encoding techniques using Hadamard or wavelet basis functions which have reconstruction algorithms with a potential complexity of $O(N^2)$ flops. This reduction in the computational complexity amounts to several orders of magnitude reduction in the reconstruction time with PFI. The main reason for this reduction is the special structure of the PFI basis functions which allows the use of the fast Fourier transform (FFT).

The performance of PFI in the presence of B_0 inhomogeneity can also be easily understood. Since the slice profile is the same for all excitations, the associated gradient strength is uniform all along the experiment time. Given that the B_0 inhomogeneity effect depends mainly on the gradient strength and that the reconstruction process involves only Fourier transformations, the effect of magnetic field inhomogeneity will be very similar to that encountered with Fourier imaging. The stronger the field gradient, the less the image distortion resulting from the magnetic field inhomogeneity becomes.

In experimental studies described in this paper, a small flip angle is used to avoid the nonlinearity effect of the RF pulse which is evident in the calculated excitation profiles. In principle, the nonidealities of the excitation profile can be corrected for by inverse filtering in PFI, and the use of low flip angles is not necessary. Nevertheless, the inverse filter may not be desirable as it leads to a lower acquisition efficiency and some loss in the SNR. At this point, a full analysis of the performance of PFI as a function of flip angle has not been performed. Such an analysis will be beneficial in the optimization of PFI.

VIII. CONCLUSIONS

The theory and experimental verification of a novel spatial encoding technique, PFI, was presented. The new technique is based on a uniform sampling of the phase-space plane on a Gabor grid and allows for controlled mixing of selective excitation and Fourier encoding. The technique has potential applications in many areas such as volume imaging, magnetic resonance angiography, and dynamic imaging.

ACKNOWLEDGMENT

The authors would like to thank the anonymous reviewers for their helpful comments and suggestions which improved the readability of this paper.

REFERENCES

- [1] D. L. Parker, C. Yuan, and D. D. Blatter, "MR angiography by multiple thin slab 3-D acquisition," *Magn. Reson. Med.*, vol. 17, pp. 434–451, 1991.
- [2] D. M. Healy, Jr. and J. B. Weaver, "Two applications of wavelet transforms in magnetic resonance imaging," *IEEE Trans. Inform. Theory*, vol. 38, no. 2, pp. 840–860, 1992.
- [3] G. P. Zientara, L. P. Panych, and F. A. Jolesz, "Dynamically adaptive MRI with encoding by singular value decomposition," *Magn. Reson. Med.*, vol. 32, pp. 268–274, 1994.
- [4] R. J. Duffin and A. C. Schaeffer, "A class of nonharmonic Fourier series," *Trans. Amer. Math. Soc.*, vol. 72, pp. 341–366, 1952.
- [5] A. I. Zayed, *Advances in Shannon's Sampling Theory*. London, U.K.: CRC, 1993.
- [6] D. Gabor, "Theory of communication," *J. Inst. Electr. Eng.*, London, vol. 93, no. III, pp. 429–457, 1946.
- [7] P. P. Vaidyanathan, *Multirate Systems and Filter Banks*. Englewood Cliffs, NJ: Prentice-Hall, 1993.
- [8] I. Daubechies, "The wavelet transform, time-frequency localization and signal analysis," *IEEE Trans. Inform. Theory*, vol. 36, no. 5, pp. 961–1005, 1990.
- [9] E. T. Jaynes, "Matrix treatment of nuclear induction," *Phys. Rev.*, vol. 98, no. 4, pp. 1099–1105, 1955.
- [10] J. J. van Vaals, M. E. Brummer, W. T. Dixon, H. H. Tuithof, H. Engels, R. C. Nelson, B. M. Gerety, J. L. Chezmar, and J. A. den Boer, "Keyhole method for accelerating imaging with contrast agent uptake," *J. Magn. Reson. Imag.*, vol. 3, pp. 671–675, 1993.
- [11] X. Hu and T. Parrish, "Reduction of field of view for dynamic imaging," *Magn. Reson. Med.*, vol. 31, pp. 691–694, 1994.
- [12] L. P. Panych and F. A. Jolesz, "Adaptive imaging algorithm for wavelet-encoded MRI," *Magn. Reson. Med.*, vol. 32, pp. 738–748, 1994.
- [13] L. P. Panych, P. D. Jacob, and F. A. Jolesz, "Implementation of wavelet-encoded MR imaging," *J. Magn. Reson. Imag.*, pp. 649–655, 1993.
- [14] L. P. Panych, C. Oesterle, G. P. Zientara, and J. Hennig, "Implementation of a fast gradient-echo SVD encoding technique for dynamic imaging," *Magn. Reson. Med.*, vol. 35, pp. 554–562, 1996.
- [15] J. Frahm, A. Haase, and D. Matthaei, "Rapid three-dimensional MR imaging using the FLASH technique," *J. Comput. Assist. Tomogr.*, vol. 10, no. 2, pp. 363–368, 1986.